Cortical Visual Processing Differences in Myopia and Blur

Katia Steinfeld[1,2,*], Micah M. Murray[1,2]

[1]The Radiology Department, Lausanne University Hospital and University of Lausanne, 1011, Lausanne, Switzerland

[2]The Sense Innovation and Research Center, 1007, Lausanne and Sion, Switzerland

Corresponding author: katia.steinfeld@unil.ch

The authors declare no competing financial interests.

Abstract

Purpose: Myopia is projected to impact over 50% of the global population by 2050. However, we currently know little of the consequences of myopia on visual brain functions. Theoretical models point to a key role of optical blur in myopia's natural history. Moreover, myopia is linked to long-lasting changes in cortical visual areas. We thus hypothesized that adults suffering from moderate myopia process visual stimuli under optical blur differently than emmetropic adults.

Methods: Emmetropes (*n*=12, males *n*=3, females *n*=9) and low to mild myopes *(n*=13, males *n*=4, females *n*=9) were tested in the condition of -3 diopters of lens-induced blur. Participants performed an illusory contour recognition task while high-density EEG was recorded and analyzed using an electrical neuroimaging framework.

Results: We provide evidence for cortical processing differences between emmetropes and mild myopes – both of whom were tested under -3D of defocus. From topographic modulations it followed that emmetropes and mild myopes engage (partially) distinct networks of brain regions. Source estimations localized these differences to the medial portion of the occipital pole. Moreover, the predominant topography of the VEP during this period not only correlated with SRE, but also was an excellent classifier of myopia vs. emmetropia. By contrast, our analyses provided no evidence for differences in visual completion processes.

Conclusions: To our knowledge, this is the first study of myopia pairing high density EEG and a behavioral task. Collectively, this pattern of findings supports a model of myopia wherein low-level visual cortices are impacted at relatively late post-stimulus processing stages**.**

Text

Introduction

By 2050, myopia's prevalence is expected to reach 52% of the global population [1]. For effective prevention and treatment, it is essential to characterize myopia's downstream chain of events [2]. Defocus and its neural translation [3] play a central role in myopia. Myopia onsets when the eyes continue to grow past their focal distance [4]. It is most diagnosed in late childhood [5] and progresses during developmental states when neural pathways remain particularly plastic [6].

In myopia, defocus and eye growth are interrelated. Animal models have shown that induced retinal blur triggers eye elongation [7]. Furthermore, in both corrected myopic adults and children, there is significant impairment in paracentral retinal processing [8–10]; the magnitude of which correlates with myopia's progression [11]. Retinal blur is thus part of a feedforward loop of eye elongation, which results in a lifetime impairment in foveal responses [12–14].

There is also nascent evidence for lifetime changes in the brains of myopic patients, both with low (LM) and high myopia (HM), i.e. below and above -6D, respectively [15]. Cheng et al., 2020, describe a significant decrease in LM subjects' resting-state activity in V1 and the optic radiations, when compared to HM patients and emmetropes. Others have documented decreased connectivity within higher-order visual cortices in the right para-hippocampal gyrus of LM and HM individuals versus emmetropes [16]. The collective implication is that myopia impacts both lower-order and higher-order visual regions.

To our knowledge, the cortical consequences of myopia have never been investigated with high-density EEG methods and an electrical neuroimaging analysis pipeline. The technique provides (sub) millisecond temporal resolution, allowing for precise characterization of both the amplitude and the topography of cortical activity over time during a visual task [17,18]. These robust EEG analyses have produced invaluable knowledge in sensory processing [19–22] and pathologies [23–27]

Additionally, myopia and its defocus alter visual experiences during years when children are still fine-tuning their visual system. Illusory contour (IC) sensitivity, for one, matures through adolescence [28,29]. These processes allow an individual to perceive fragmented elements as continuous surfaces and unobstructed objects [30]. During childhood it involves a distributed network over occipital and frontal cortices, in a relatively effortful process [28,29]. With visual experience, the processing of such illusions gains in speed and is

consolidated over the ventral visual stream associated with object processing [31–33]. As such, one can postulate that the defocus experienced over a lifetime in adults with myopia may cascade to impact filling-in processes.

Recent evidence points to long-lasting changes in both retinal and cortical dynamics in myopia. Furthermore, defocus seems to play a central part in myopia's progression. Here, we characterize the dynamics of the interaction between myopia and optical blur in the cortex. We hypothesized that adults with low and moderate myopia process optical blur differently than emmetropic adults. To test this hypothesis, we used an illusory contour recognition task with acquiring high-density EEG recordings. To our knowledge, there have been no similar brain imaging/mapping studies of visual function that compared myopic participants with corrected-to-normal vision and emmetropic participants (though see [34] for a behavioral study of children with residual myopia following removal of congenital cataracts). As such, mechanistic differences in the processing of illusory contours remain undefined. Because we hypothesized optical blur has different effects in myopia's and emmetropia's visual processing, all participants were tested under the same level of induced defocus.

Methods

Participants

Participants underwent an orthoptic evaluation, including automated refraction, subjective refraction, and ocular motility testing. Exclusion criteria were history of neurologic, psychiatric, or ophthalmic disease, corrected visual acuity less than 0.00 LogMar in any one eye, or astigmatism equal or superior to -1D in any one eye. Two participants were excluded based on such criteria. One for high astigmatism and the other for having undergone myopia-correction surgery. Additionally, one myopic participant received an updated prescription with which they reached 0.00 LogMar visual acuity, worn during the experiment. Twenty-five participants were tested, 13 myopes (males *n*=4, females *n*=9) and 12 emmetropes (males *n*=4, females *n*=9). Because there were no significant differences in spherical equivalent of refractive error between each subjects' eyes and none of the subjects were hyperopic (see *Participants*), we refer to the refractive error as the absolute value of the mean between both eyes' spherical equivalent (sphere + cylinder/2). The Cantonal Ethics Committee approved this project (protocol #2018-00240). All participants provided written informed consent after verbal and written explanation of the study, according to the tenets of the Declaration of Helsinki.

Stimuli and Paradigm

Participants sat at 60cm distance from a 20-inch LCD monitor, 1600 x 1200 @ 60Hz, pixel response time 16ms, display 100 PPI. Emmetropia group wore only one frame with +3D convex lenses. Participants had both eyes un-occluded. During breaks they were allowed to take off the frames and were advised to close their eyes to avoid fatigue. For the experiments, participants viewed five stimuli: a dartboard, two illusory contour shapes (Ics) and two non-illusory contour (NC) images.

The IC stimuli were Kanizsa-style squares and circles formed by four 'pacman' inducers. Each pacman's diameter was 6.96° of visual angle. The IC square (IC_s) sides subtended 9.52° of visual angle with a support ratio of 50%. ICS inducers were presented on the diagonal axes with their centers at 11.18° of eccentricity from central fixation. The IC circle's (IC_c) diameter subtended 10.76° of visual angle with a support ratio of 62%. ICC inducers were presented on the cardinal axes with their centers at 8.54° of eccentricity from central fixation. The no-contour (NC) circle (NC_C) and square (NC_S) inducers were at the same position as in their IC counterparts but rotated 180° outwards. We chose to use two

illusory contour shapes formed by inducers at different positions to avoid an attentional bias, where participants would potentially complete the task by selectively attending certain regions of the visual field. Furthermore, other studies by our group have successfully used these same inducers and illusory contour shapes, providing a benchmark for IC sensitivity markers [32,35].

Participants' task was to indicate the presence vs. absence of an illusory contour, regardless of its shape, via a serial response box (see also [32]). Subjects were instructed to press a button labeled '1' as quickly and accurately as possible when they saw a shape, either circle or square, and another button label '2' when they did not. In turn, participants were instructed not to respond to the dartboard stimulus. There were no restrictions regarding hand preference. One participant in the myopia group, and two participants in the emmetropia group responded with their left hand.

The dartboard was a circular, black, and white, pattern-reversal stimulus. Its Michelson contrast was 100%. It consisted of 16 wedges and 8 concentric circles or a total of 128 checks. The eight concentric circles had eccentricities of 1.60°, 3.32°, 4.83°, 6.44°, 8.05°, 9.64°, 11.24° and 12.84°. Spatial frequencies within wedges were of 0.3 cpd. Spatial frequencies at the border of each ring ranged from 0.8 cpd (innermost) to 0.1 cpd (outermost). Within this eccentricity and spatial frequency range at this contrast, resolution is not a constraint. Every presentation lasted 400ms and reversed in spatial phase at 5Hz (10 reversals per second, 100ms for each pattern). Data in response to these stimuli were not the focus of the present study and thus will not be treated further here.

The complete sequence is depicted in Figure 1. It consisted of a dartboard presentation for 400ms followed by a blank interval of 1s on average (random duration ranging 0.8-1.2s), a subsequent pacman array presentation for 400ms, and a second blank interval of 2s on average (random duration ranging 1.8-2.2s). Stimulus order of ICs and NCs within a block was pseudo-randomized. A block of trials lasted 6min on average and included 80 dartboard presentations interleaved with 80 pacmen array stimuli (i.e., 40 IC and 40 NC stimuli). Participants underwent one training session prior to recording and ≥8 recorded blocks of trials.

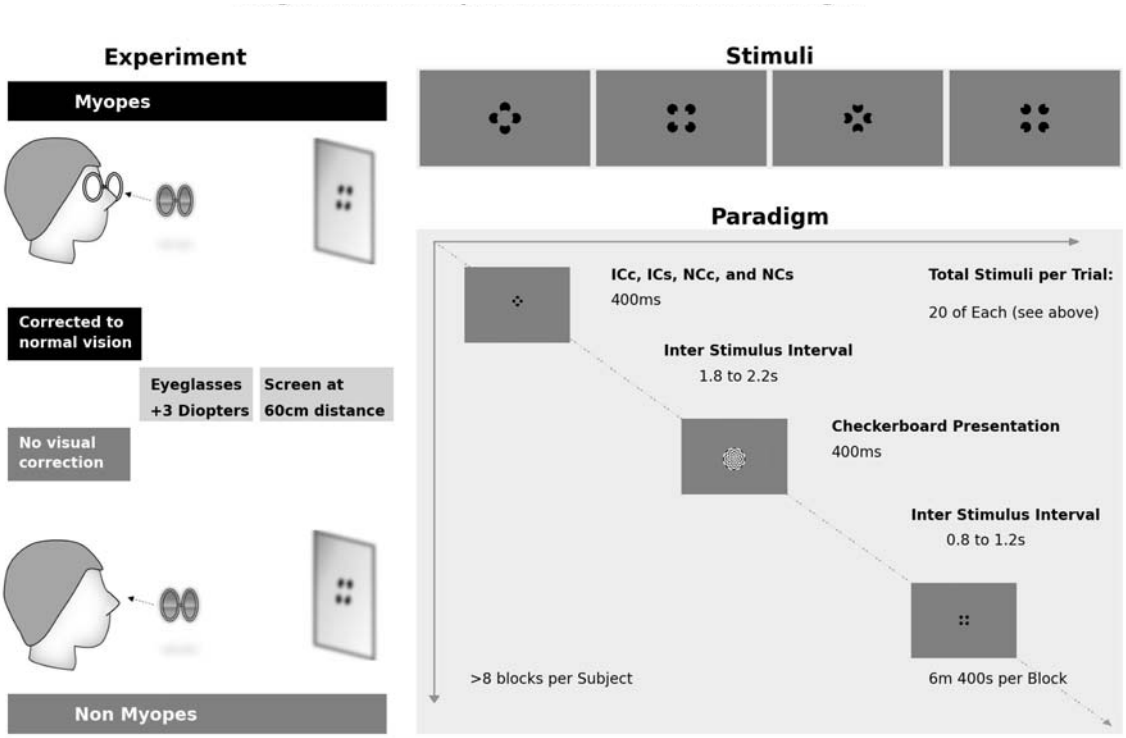

Figure 1 – Diagram of the Experiment, Stimuli and Paradigm.

Behavioral Analyses

Subjects and trials excluded from the analysis according to EEG criteria were also excluded from the behavioral analyses. We exported the behavioral dataset as pandas in Python for calculation of mean reaction times, error rates and false alarm rates. An 'error' was computed when participants reported seeing an illusory shape when an NC stimulus was presented. A 'false alarm' was counted when participants reported seeing a contour during a time window where none of the illusory contour conditions were present, neither IC nor NC, for instance during a dartboard presentation. False alarm rates were below 1% for myopes and emmetropes; thus they were not examined. A mixed-model repeated measures ANOVA was performed with the SPSS software [36], with Stimulus (IC vs. NC) as the within-subjects factor and Group (myopia vs. emmetropia) as the between-subjects factor.

EEG Acquisition and Preprocessing

Continuous EEG was acquired at 1024Hz through a 128-channel Biosemi ActiveTwo AD-box referenced to the common mode sense (CMS; active electrode) and grounded to the driven right leg (DRL; passive electrode). This configuration creates a feedback loop, driving

the montage's average potential towards the amplifier zero. We used the Cartool freeware [37] for pre-processing and analyses. The continuous EEG was filtered with a Butterworth filter (−12dB/octave roll-off, High pass 0.18Hz, Low pass 60 Hz), underwent DC/0 Hz removal and were notched at 50Hz. Epochs spanned from 100ms pre-stimulus onset to 500ms post-stimulus onset. All epochs were then tested to the threshold value of ±80μV, in a semi-automated fashion accompanied by visual inspection, to reject epochs with artifacts and transient noise. Epochs were then averaged to create Visual Evoked Potentials (VEPs) for each subject and stimulus.

Subsequently, all epochs from one subject and stimulus were averaged, creating VEPs. VEPs were then 40Hz low-pass filtered. To identify electrodes that were broken or consistently had bad contact, VEP waveforms (calculated against the original and common averaged reference) and topographies were inspected. Signal from each selected electrode was replaced by an interpolation (Mean±SD= 7.36±4.11 electrodes, *max*=14*, min*=0) using three-dimensional splines [38]. During this pre-processing, 5 participants were excluded due to excessive noise. Results presented here are thus based on data from 13 myopes and 12 emmetropes. For each of these remaining participants, more than 150 epochs were accepted in response to each stimulus condition (i.e. IC_C, IC_S, NC_C, and NC_S; Mean±SD= 597±107 epochs). As our interest here was not in the responses to individual stimulus conditions, we collapsed IC_C and IC_S epochs into a single IC VEP for each participant. There were no significant differences in the final number of accepted epochs per condition ($F_{(1,19)}$ =0.2498, p=0.128, η_p^2 =0.098) or between groups ($F_{(1,23)}$ =0.654, p=0.427, η_p^2 =0.028).

VEP Analyses

VEP analyses followed a 2×2 mixed model design with the between-subjects factor of Group (myopia vs. emmetrope) and the within-subjects factor of Stimulus (IC vs. NC). For the analysis of voltage waveforms and GFP waveforms, we used the freeware [39]. Both the VEP waveforms from the full electrode montage as well as reference-independent measures of the electric field at the scalp were analyzed [17,40]. Statistical effects on VEP waveforms needed to meet both a temporal criterion of ≥10 contiguous time points as well as a spatial criterion of spanning across at least 10% of the electrodes [19,41]. In terms of reference-independent measures, we first analyzed the global field power (GFP), which is the root mean square of the voltage of all electrodes and yields larger values for stronger VEPs. When analyzing GFP, significant main effects or interactions needed to satisfy a temporal criterion of ≥10 contiguous time points.

The VEP topography, which is also reference-independent, was analyzed with hierarchical clustering and application of a modified Krzanowski-Lai criterion to select the

number and pattern of stable VEP topographies that best characterized the variance in the concatenated dataset [42]. This technique maps stable electric field topography, or 'template maps', across time for each group and stimulus condition. By visual inspection of the clustering results, periods when 'template maps' differed between groups and/or stimulus conditions were determined. All further steps were constricted to each of these time periods, considered separately.

To statistically assess potential topographic differences during these time periods, individual subject's VEPs were fitted with all the 'template maps' identified in these time periods. This fitting procedure entails labelling each time point with the template map with which it best correlates spatially [42]. As an output, it yields the total number of time points a given template map fit the data from each subject and stimulus. These values were then submitted to an rmANOVA. This rm-ANOVA had as within-subjects factors of 'template maps' as well as Stimulus (IC vs. NC) and the between-subjects factor of Group (myopia vs. emmetropia). We also performed a linear regression between the template maps' total number of time points with refractive error.

Lastly, source reconstruction was performed for the time periods where clustering results showed a significant difference between Groups and/or Stimuli or their interaction. Firstly, VEPs for each subject were averaged across IC and NC conditions (as only a main effect of Group was observed, as detailed below), cropped to the selected time window and averaged over time. Source modelling was performed with a distributed linear inverse solution (minimum norm) combined with the LAURA (local autoregressive average) regularization approach ([43,44] ; see also [45] for a comparison of inverse solution methods). The solution space was calculated on a realistic head model that included 5923 nodes, selected from a grid equally distributed within the grey matter of the Montreal Neurological Institute's average brain (available from https://sites.google.com/site/cartoolcommunity/downloads). The head model and lead field matrix were generated with the Spherical Model with Anatomical Constraints (SMAC; Spinelli et al., 2000 as implemented in Cartool version 4.10 [37] using a 4-shell model (skull, scalp, cerebral spinal fluid, and brain) as well as with an upper skull thickness (5.7mm) and mean skull conductivity (0.021S/m) values based on the mean age of our sample. As an output, LAURA provides current density measures; their scalar values were evaluated at each node. Statistical analysis of source estimations was performed with an un-paired t-test ($p<0.05$ at a given node) and with a spatial extent criterion of minimally 10 contiguous nodes based on randomization thresholds (see also [20,30,35,47,48] for similar implementations).

Results

Demographics and refraction

The myopia and emmetropia groups did not differ in age ($t_{(23)}$=0.68; p =0.51; d=0.27), sex ($X^2_{(1,\ 25)}$= 0.33; p=0.57) or years of education ($t_{(23)}$=1.19; p =0.97; d=.48). All myopia patients were first diagnosed between the ages of 12 and 21 years, which was ≥8 years prior to this study (range=8-28 years; mean±SD=14.23±1.69 years). For all participants, between-eyes differences in sphere (SRE) and cylinder (CRE) refractive error were not clinically relevant (difference in SRE ≤ |1.25|D, in CRE ≤ |0.25|D). In an rm-ANOVA of astigmatism levels where within subjects factor were right and left eyes and between subjects factor were myopia and emmetropia groups, astigmatism was shown to be significantly higher ($F_{(1,23)}$=7.246; p=0.013; η_p^2 =0.24) in the myopia group (mean±SD in the right eye =-0.462±0.105 and -0.481±0.098 in the left eye) than in the emmetropia group (right eye =-0.083±0.109; left eye =-0.104±0.102). There were no significant differences in astigmatism levels between eyes for either group ($F_{(1,23)}$=0.23; p=0.63; η_p^2 =.010).

For all 25 participants, we calculated the spherical equivalent from each eye's sphere and cylinder refractive errors, averaged the spherical equivalents of both eyes and took its absolute value, thus obtaining a unique positive average spherical equivalent value per subject (SRE). Myopia was present in 13 participants (SRE ranged -3.69D to -1.36D; mean±SD = -1.36±1.38D) and absent in 12 participants (SRE ranged -1D to 0D; mean±SD = -0.34±0.28D). For a complete description of myopes' and emmetropes' refractive errors see Supplementary Table S1 and S2 respectively in supplementary data.

Table 1 - Participant's Average Of Both Eyes' Spherical Equivalent, Age of Diagnosis, Age, Years With Correction, Years Of Tertiary (Post-secondary School) Education And Sex.

Myopia Group						*Emmetropia Group*			
Avg SRE	*Age at Diagnosis*	*Age Range*	*Years with Correction*	*Years of Tertiary Education*	*Sex*	*Avg SRE*	*Age Range*	*Years of Tertiary Education*	*Sex*
-2.063	12	26-30	15	7	M	.250	26-30	4	M
-3.688	14	21-25	10	5	M	-.313	26-30	6	M
-1.813	17	31-35	15	4	F	.000	21-25	4	M
-3.125	12	36-40	25	8	F	-.625	26-30	5	F
-3.375	10	26-30	17	6	F	-.500	26-30	5	F
-2.625	16	21-25	9	5	F	.000	26-30	5	F
-1.063	14	26-30	12	3	F	.000	26-30	4	F
-2.688	15	21-25	8	4	F	.000	26-30	5	M
-2.813	10	21-25	13	4	F	.000	21-25	5	F
-1.438	21	31-35	12	6	M	-.125	16-20	2	F
-2.625	12	36-40	28	9	F	-.125	36-40	9	F
-1.625	16	21-25	8	5	F	.000	16-20	1	F
-2.125	12	21-25	13	5	F				
Group average	*Age at Diagnosis*	*Age in years*	*Years with Correction*	*Years of Tertiary Education*	*Sex*	*Avg SRE*	*Age in years*	*Years of Tertiary Education*	*Sex*
-2.390	13.9	28.2	14.2	5.5	10F/3M	-0.120	26.7	4.6	8F/4M

Behavioral Results

All participants performed at or above 87% accuracy on the illusory contour recognition task. False alarms represented >1% of the trials for four participants. When false alarm rates were analyzed with a 2×2 rmANOVA, there was no evidence of a main effect of Group or Stimulus nor any interaction (all p's >0.34). There was no evidence of reliable differences between groups in terms of accuracy ($F_{(1,23)}$=0.010; p =0.920; η^2 =0.00) or reaction times ($F_{(1,23)}$ = 0.48; p =0.83; η_p^2 =0.002). There was a main effect of Stimulus on reaction times ($F_{(1,23)}$=11.721; p =0.002; η_p^2 =0.338), with detection of ICs being significantly faster than that of NCs (mean±SD = 466±17ms vs. 500±17ms). However, accuracy was not significantly different between stimulus conditions ($F_{(1,23)}$=0.763; p=*0.391*; η_p^2 =0.032). The interaction term was not significant for either the analysis of accuracy rates ($F_{(1,23)}$=1.261; p=0.273; η_p^2=0.052) or reaction times ($F_{(1,23)}$=0.678; p=0.419, η_p^2=0.029). To investigate possible speed-accuracy trade-offs, we computed inverse efficiency scores, i.e. mean reaction times divided by percentage of correct trials [49,50]. The rmANOVA on inverse efficiency scores did not reveal a significant effect of Group ($F_{(1,23)}$=0.055; p=0.816; η_p^2=0.002) nor a significant Group × Stimulus interaction ($F_{(1,23)}$=1.194; p=0.286; η_p^2=0.049). The significant main effect of Stimulus did, however, persist ($F_{(1,23)}$=5.907; p=0.023; η_p^2=0.204), confirming that the speed gain in IC detection did not come at the cost of accuracy.

Neurophysiological Results

Illusory Contour Sensitivity

In light of our prior work on brain mechanisms of illusory contour sensitivity in adult humans [32,35,51–58], we anticipated that responses to the IC and NC conditions would differ, with initial effects peaking at ~150-170ms post-stimulus onset (reviewed in [59]). Exemplar VEP and GFP waveforms are displayed in Figure 2 and show that indeed responses were enhanced to the IC vs. NC condition in both groups. This was statistically assessed by the main effect of Stimulus in the 2×2 rmANOVA on VEP and GFP waveforms and by subsequent paired t-tests within each group. More specifically, analysis of VEP voltage waveforms revealed a significant main effect of Stimulus over three post-stimulus time periods: 138-248ms (all $F's_{(1,23)} \geq 0$; $p \leq 0.05$), 292-329ms (all $F's_{(1,23)} \geq 0$, $p \leq 0.05$), and 350-496ms (all $F's_{(1,23)} \geq 0$, $p \leq 0.05$). Likewise, analysis of Global Field Power revealed a main effect of Stimulus over similar time periods: 145-203ms ($F_{(1,23)} \geq 4.78$, $p \leq 0.04$), 254-271ms ($F_{(1,23)} \geq 4.56$, $p \leq 0.05$), and 343-455ms ($F_{(1,23)} \geq 4.37$, $p \leq 0.05$). In all cases, GFP was

stronger to IC than to NC stimuli (Figure 2). By contrast, there was no evidence of reliable interactions of Stimulus on Group. Topographic clustering provided no indication of any main effect of Stimulus nor interaction involving this factor. Consequently, we focus below on the main effect of Group and interactions involving that factor, as such indicates visual processing differences between myopes and emmetropes.

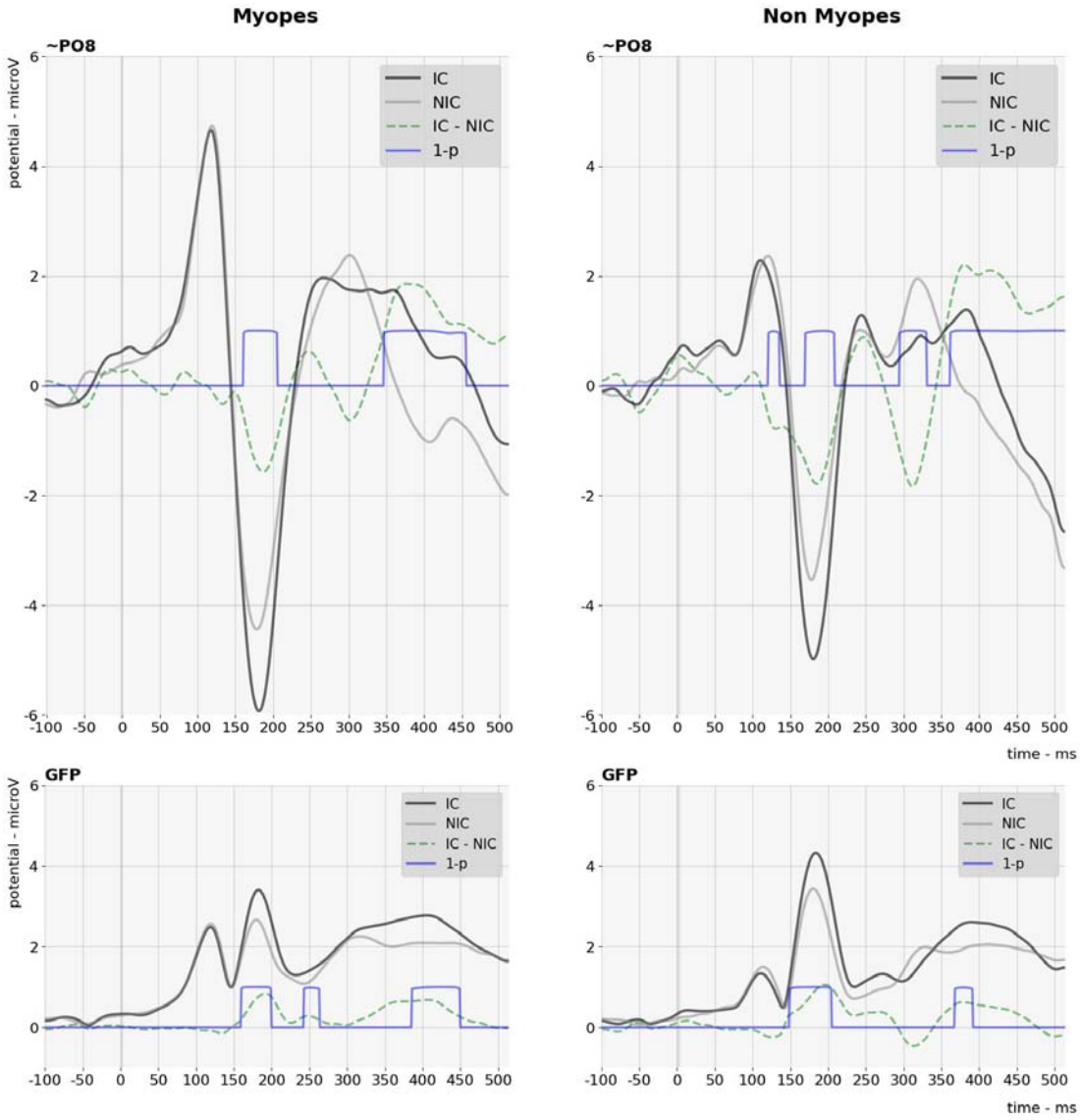

Figure 2 – Waveforms And Global Field Power (GFP) Of Electrical Activity At Occipital Electrodes.

Group-Wise Differences in Visual Processing

In addition to the main effect of Stimulus, the rmANOVA on VEP waveforms revealed a main effect of Group over the 240-290ms post-stimulus onset period ($p<0.05$). The analysis of GFP waveforms provided no evidence for a significant main effect of Group. By contrast, the topographic clustering of the group-averaged data identified a period spanning 223-287ms post-stimulus onset when 3 template maps characterized the data, which we refer to as map2, map3 and map4 (Figure 3). One of these three template maps appeared to be common to both groups (map2), whereas map3 and map4 appeared to characterize responses from different groups. The single-subject fitting procedure was performed over the 223-287ms post-stimulus period with all three template maps and revealed a significant Group × Template Map interaction ($F_{(1,23)}$=6.868; p=0.005; η_p^2 =0.384). To better understand the bases for this interaction, follow-up ANOVAs were conducted for each template map separately. For map2, there was no evidence for group-wise differences ($F_{(1,23)}$=2.582; p=0.122; η_p^2=0.101). By contrast, both map3 and map4 exhibited main effects of Group (($F_{(1,23)}$=7.336; p=0.013; η_p^2=0.242) and ($F_{(1,23)}$ =9.3; p=0.005; η_p^2=0.290), respectively). More specifically, map3 better characterized responses from myopes than from emmetropes (mean±SD = 11.1±2.8ms vs. 0.3±2.9ms), and map4 better characterized responses from emmetropes than from myopes (mean±SD = 41.0±5.6ms vs. 17.2±5.4ms). Collectively, these results indicate that responses of myopic individuals result in different topographies of the electric field at the scalp, and by extension different configurations of intracranial sources, than their emmetropic counterparts.

Next, we tested whether the preponderance of map3 and/or map4 was correlated with the extent of refractive error (quantified here by SRE). There was a significant correlation when data were pooled across groups, both when testing the duration of map3 and map4 (($F_{(1,23)}$=10.121; p =0.004; r^2=0.275) and ($F_{(1,23)}$=17.522; p <0.001; r^2=0.408), respectively). We furthermore assessed to what extent the VEP topography could reliably classify an individual as myopic, using the area under the ROC curve. For the duration of map3, the accuracy obtained was acceptable (*AUC*=0.760; *SD*=0.101; p=0.010 and an overall model quality estimated at 0.56). For the duration of map4, the accuracy was good (*AUC*=0.817; *SD*=0.087; p<0.001 and overall model quality estimated at 0.67). By way of comparison (and as expected), SRE proved to be a perfect predictor (AUC=1.00; *SD*=0.000, p<0.0001 and overall model quality estimated at 1.00) (Figure 3).

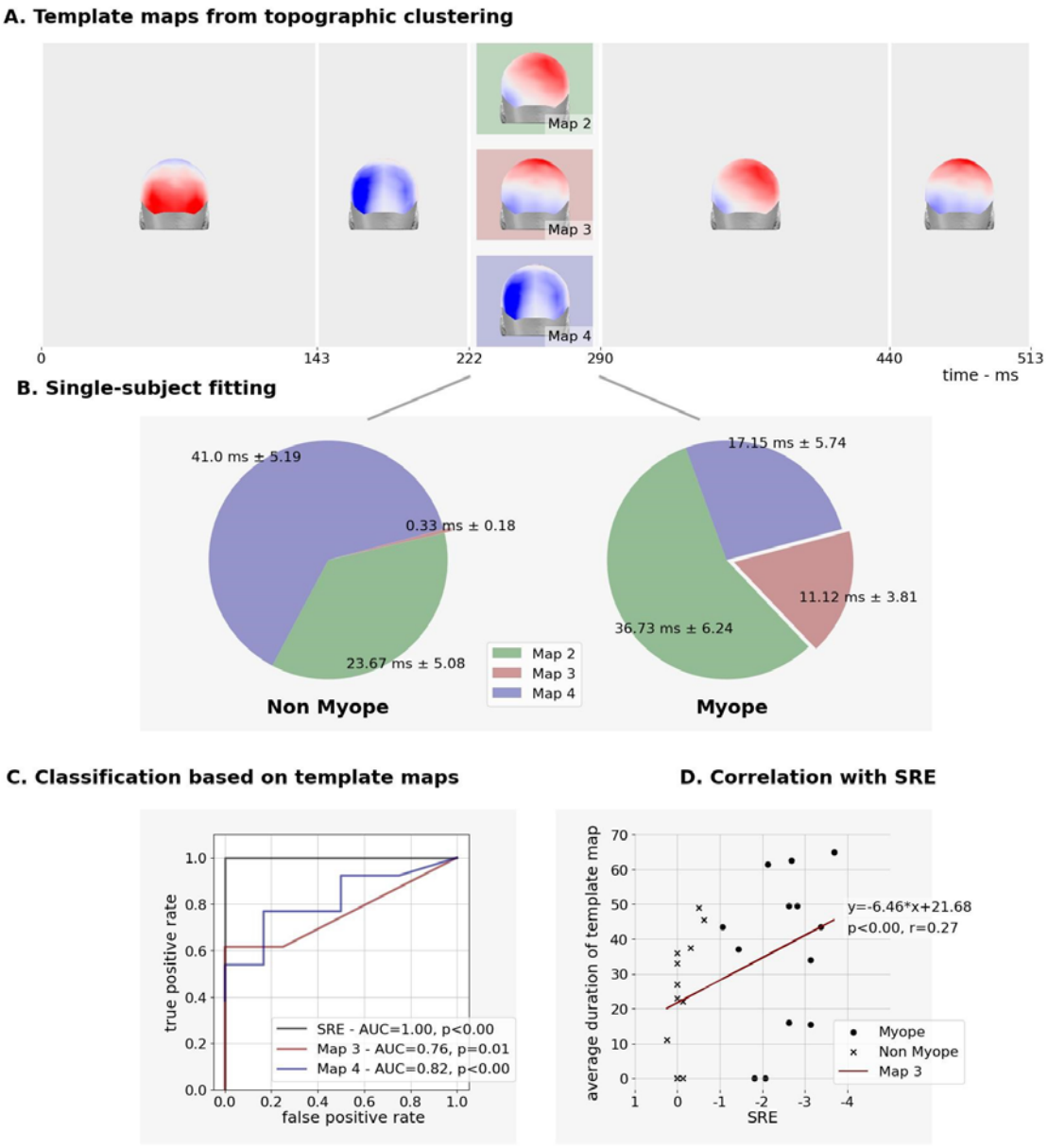

Figure 3 – Group Differences in Duration of Stable Topographies.

Finally, we performed source estimations over the 223-287ms post-stimulus period to compare groups after collapsing data across stimulus conditions (Figure 4). Robust sources were observed along the medial portion of the occipital pole as well as lateral occipital and inferior temporal cortices bilaterally. The statistical contrast of these source estimations revealed stronger responses from myopes within the medial portion of the occipital pole. Stronger responses from emmetropes were observed within inferior frontal and parietal cortices. However, these were diffuse and did not meet our spatial extent criterion.

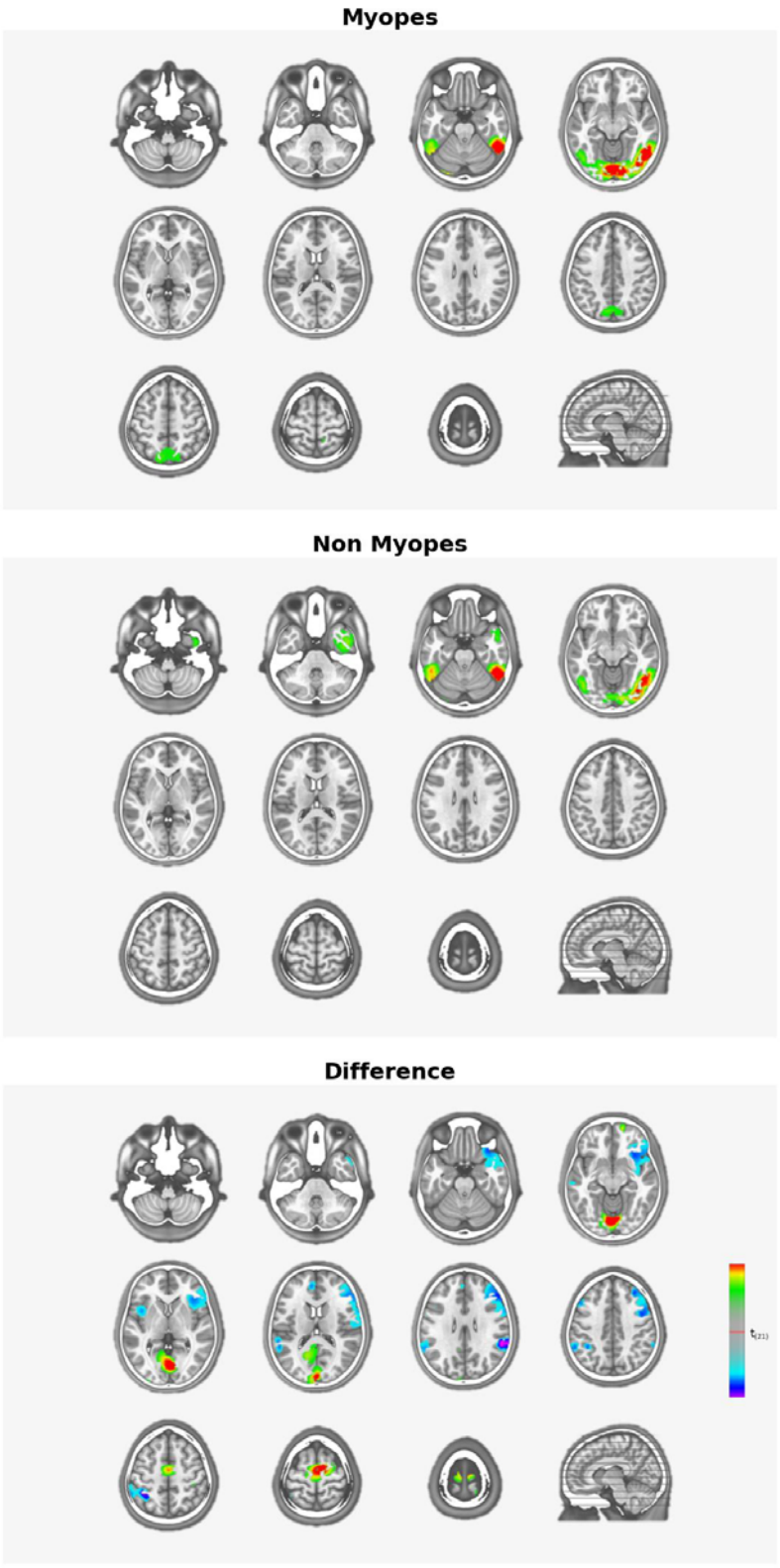

Figure 4 – Source Reconstruction (222 to 290ms).

Discussion

We provide evidence for general cortical processing differences between emmetropes and mild myopes – both of whom were tested under -3D of defocus – that manifest over relatively late post-stimulus periods. That these differences followed from topographic modulations indicates that emmetropes and mild myopes engage (partially) distinct networks of brain regions. Our source estimations and analyses thereof localized these differences to the medial portion of the occipital pole, with stronger source activity for myopes than emmetropes. Moreover, the predominant topography of the VEP during this period not only correlated with SRE, but also was an excellent classifier of myopia vs. emmetropia. By contrast, our analyses provided no evidence for differences in visual completion processes; task performance as well as the neural correlates of visual completion were similar in both groups. Collectively, this pattern of findings supports a model of myopia wherein low-level visual cortices are impacted at relatively late post-stimulus processing stages, perhaps indicative of altered attentional processes and/or susceptibility to visual fatigue.

Using Kanizsa-type illusory contours, we assessed participants' abilities to perform visual completion. There was no evidence for group differences in behavior. Rather, performance accuracy was at near ceiling levels, and reaction times were generally faster for IC than NC stimuli in both groups. This pattern suggests that perceptual completion is functionally intact despite blur and myopia. In agreement, McKynton et. al. [34] assessed both low-level and mid-level visual functions in sighted and cataract-treated children. The sighted children were presented with blurred versions of stimuli to emulate the visual acuity of cataract-treated children. The performance of the sighted children presented with blurred stimuli was at near-ceiling levels, like what we observed here. By contrast, performance of cataract-treated children was significantly lower and may reflect a long-term consequence of severe and sustained visual loss during childhood, though longitudinal follow-up of these children remains undone and would be informative regarding the full extent of functional recovery (see also [60] for similar evidence as well as [61] for results of intact IC perception despite retinal scarring in individuals with scotoma from macular degeneration). Similarly, topological perception remains unaffected in corrected-to-normal mild to high myopia [62]. Our results contribute to this topic by showing that adults with mild myopia perform visual completion in a manner indistinguishable from that of emmetropes when both groups have the same degree of blur. In agreement, studies of geometric illusions in adults with corrected-to-normal vision in the condition of optical blur also observed that the magnitude of the illusions is not affected by defocus [63,64].

Our VEP data provide additional evidence regarding the integrity of visual completion processes despite blur. Both emmetropes and myopes exhibited enhanced VEPs to the presence vs. absence of illusory contours; the first phase of which peaked at ~150-170ms post-stimulus onset (see Figure 2). This enhancement followed from modulations in response strength with no evidence for modulations in response topography. The implication is that visual completion stems from stronger responses within a statistically indistinguishable network of active brain regions. Prior works from our group and others' have likewise characterized illusory contour processes as unfolding in this manner (e.g. [32,35,51,53–59]). Of relevance here are the findings reported in Shpaner et al. [57] who compared visual completion of illusory contours and salient region stimuli (see also [65]). Salient region stimuli are comprised of "rounded" versions of the inducers (cf. Figure 1 in [57]). While not blurred, salient region stimuli have been shown to reduce the strength of perceived completion (e.g. [66]). What Shpaner et al. [57] demonstrated is that that illusory contour stimuli evoked larger responses at earlier post-stimulus latencies (i.e. ~150-170ms) than salient region stimuli, which instead evoked larger responses at later post-stimulus latencies. Such results thus differentiate between completion-related effects from the two varieties of stimuli. Our findings here can thus be situated alongside these to support an interpretation wherein robust illusory contour completion occurs during the ~150-170ms post-stimulus period and despite the presence of -3D blur.

Our principal finding is the presence of general visual processing differences between myopes and emmetropes under -3D of defocus. Two aspects are particularly noteworthy. On the one hand, the timing of these effects at ~240ms post-stimulus onset is relatively protracted. On the other hand, group-wise differences followed from topographic rather than strength modulations, indicative of changes in the configuration of the active brain networks. Moreover, source estimations localized differences to medial regions of the occipital pole within primary visual cortices (see Figure 4). The timing of the group-wise differences is roughly 200ms later than reports of cortical response onset, which has been shown to occur at ~50ms post-stimulus onset in response to high contrast stimuli (e.g. [32,67,68]). Moreover, these group-wise differences follow the initial stages of visual completion, which typically peak at ~150ms post-stimulus onset as described above. The timing of the present differences at ~240-290ms instead coincides with reports of periods of more effortful visual completion and visual perception (e.g. [28,53,55,69–72]). For example, Sehatpour et al. [72] compared brain responses to scrambled and unscrambled drawings of common objects. They observed VEP modulations over the ~230-400ms consistent with the so-called N_{cl} or negativity for closure that was originally characterized by Doniger et al.[70]. Consistent with an interpretation in terms of effortful object recognition, there is evidence that this effect shifts

earlier in time, i.e. peaking at ~150-170ms, when the to-be-recognized object has been recently identified [71]. Our results are similar insofar as the group-wise differences reflect changes in the cortical networks recruited by myopes and emmetropes to perform visual completion. More specifically, responses from our myopic participants included prominent sources within lateral occipital as well as primary visual cortices, whereas source estimations from emmetropic participants were limited to lateral occipital cortices (Figure 4). Although the literature is inconsistent with regard to whether structural alterations in myopia impact gray versus white matter, evidence consistently points to effects within low-level visual cortices along the calcarine sulcus in high myopia (e.g. [73,74]). In mild myopia, alterations in resting-state cortical dynamics have been described in the optic radiations [75] and outside of visual cortices [16], persisting after refractive surgery [76].

Our findings contribute to this line of results by showing that myopic participants more prominently engage lower-level cortices under conditions of equivalent defocus. Aligned with this result are reports that myopic individuals retain better contrast sensitivity, visual acuity and reading abilities than emmetropic participants in defocus [77–79]. It will therefore be of interest to ascertain potential links more finely between activity in low-level cortices and functional abilities in myopia. Likewise, it will be important to determine the full extent to which visual processing differences, like those we report here, have been obfuscated in prior studies of visual completion, such as those cited above, because any myopic participants are typically tested while wearing their corrective lenses and in the absence of defocus. More generally, future research will likely benefit from drawing closer structural-functional relationships regarding effects involving primary visual cortices.

There is now a growing body of work comparing VEPs from myopic participants as well as from emmetropic individuals with defocus transiently induced by defocusing lenses (e.g. [80,81]). Most such studies have collected data from a limited number of scalp sites (i.e. often <3) and across a wide range of myopia severity or induced blur. While moderate and severe myopia seems to delay the latency and decrease the amplitude of VEP responses to a pattern-reversing stimulus, no reliable differences were reported between emmetropes and mild myopes (i.e. <-3D) [82]. It should be noted that these authors only considered VEP components up to ~170ms and thus did not examine post-stimulus latencies encompassing the time window here when we observed our group-wise differences. Other studies have found that blur-induced changes on VEP amplitude and latency depend on the stimuli used, with effects occurring for high but not low spatial frequency stimuli [83]. Specifically, induced blur affected pattern-reversal VEPs, but not motion-onset VEPs. In the case of the present study, the Kanizsa-type stimuli were comprised of a preponderance of lower spatial frequencies, potentially explaining (at least partially) why group-wise effects manifested only

at relatively late post-stimulus latencies. Importantly, our results also indicate that such effects are not simply the consequence of blur, as both groups viewed stimuli under identical defocus. Rather, we would contend that the differences we observed here follow from lifetime experience of mild myopia. In agreement with this interpretation is our observation of a strong correlation between the prevailing VEP topography over the 223-287ms post-stimulus period and the extent of refractive error, as measured via SRE. Moreover, the predominance of a given VEP topography was an excellent classifier of an individual as myopic or emmetropic (Figure 3).

In summary, we provide evidence that illusory contour perception and its neural correlates are indistinguishable in myopes and emmetropes who are viewing stimuli under equivalent conditions of -3D blur. Despite this similarity, we also characterize general visual processing differences between myopes and emmetropes. However, and unlike prior research, we find that these differences manifest at relatively late post-stimulus latencies and stem from topographic differences between groups. Source reconstructions indicated that myopes recruit primary visual cortices during this time, which may reflect a difference in more conceptual phases of object recognition and identification. Finally, the correlation between topographic features of the VEP and measures of refractive error suggests that there may be a direct, longstanding consequence of myopia on visual cortical function.

Acknowledgements: The Sense Innovation and Research Center is a joint venture supported by the Lausanne University Hospital (CHUV), the University of Lausanne (UNIL), and the University of Applied Sciences Western Switzerland (HES-SO Valais/Wallis). KS is supported by an MD-PhD fellowship of the Swiss Academy of Medical Sciences (Grant MD-PhD 21/21). MMM is supported by the Swiss National Science Foundation (Grant 169206). We thank Ms. Astrid Minier for their assistance in orthoptic evaluations.

References

1. Modjtahedi B, Ferris F, Hunter DG, Fong D. Public Health Burden and Potential Interventions for Myopia. *Ophthalmology*. 2018;125:628-630. doi:10.1016/j.ophtha.2018.01.033

2. Wildsoet CF, Chia A, Cho P, et al. IMI – Interventions for Controlling Myopia Onset and Progression Report. *Invest Ophthalmol Vis Sci*. 2019;60(3):M106-M131. doi:10.1167/iovs.18-25958

3. Maiello G, Walker L, Bex PJ, Vera-Diaz FA. Blur perception throughout the visual field in myopia and emmetropia. *J Vis*. 2017;17(5). doi:10.1167/17.5.3

4. Wolffsohn JS, Flitcroft DI, Gifford KL, et al. IMI – Myopia Control Reports Overview and Introduction. *Invest Ophthalmol Vis Sci*. 2019;60(3):M1-M19. doi:10.1167/iovs.18-25980

5. Chua SYL, Sabanayagam C, Cheung YB, et al. Age of onset of myopia predicts risk of high myopia in later childhood in myopic Singapore children. *Ophthalmic Physiol Opt J Br Coll Ophthalmic Opt Optom*. 2016;36(4):388-394. doi:10.1111/opo.12305

6. Atkinson J, Braddick O. Visual Development. The Oxford Handbook of Developmental Psychology, Vol. 1. doi:10.1093/oxfordhb/9780199958450.013.0010

7. Chakraborty R, Ostrin LA, Benavente-Perez A, Verkicharla PK. Optical mechanisms regulating emmetropisation and refractive errors: evidence from animal models. *Clin Exp Optom*. 2020;103(1):55-67. doi:10.1111/cxo.12991

8. Chen JC, Brown B, Schmid KL. Delayed mfERG responses in myopia. *Vision Res*. 2006;46(8-9):1221-1229. doi:10.1016/j.visres.2005.06.030

9. Gupta SK, Chakraborty R, Verkicharla PK. Electroretinogram responses in myopia: a review. *Doc Ophthalmol*. 2022;145(2):77-95. doi:10.1007/s10633-021-09857-5

10. Ho W cheung, Kee C su, Chan HH lung. Myopia Progression in Children Is Linked with Reduced Foveal mfERG Response. *Invest Ophthalmol Vis Sci*. 2012;53(9):5320-5325. doi:10.1167/iovs.12-10185

11. Luu CD, Foulds WS, Tan DTH. Features of the multifocal electroretinogram may predict the rate of myopia progression in children. *Ophthalmology*. 2007;114(8):1433-1438. doi:10.1016/j.ophtha.2006.11.030

12. Haarman AEG, Enthoven CA, Tideman JWL, Tedja MS, Verhoeven VJM, Klaver CCW. The Complications of Myopia: A Review and Meta-Analysis. *Invest Ophthalmol Vis Sci*. 2020;61(4):49. doi:10.1167/iovs.61.4.49

13. Li SZC, Yu WY, Choi KY, et al. Subclinical Decrease in Central Inner Retinal Activity Is Associated With Myopia Development in Children. *Invest Ophthalmol Vis Sci*. 2017;58(10):4399-4406. doi:10.1167/iovs.16-21279

14. Zereid FM, Osuagwu UL. Myopia and Regional Variations in Retinal Thickness in Healthy Eyes. *J Ophthalmic Vis Res*. 2020;15(2):178-186. doi:10.18502/jovr.v15i2.6735

15. Troilo D, Smith E, Nickla D, et al. IMI – Report on Experimental Models of Emmetropization and Myopia. *Investig Opthalmology Vis Sci*. 2019;60:M31. doi:10.1167/iovs.18-25967

16. Cheng Y, Yan L, Hu L, et al. Differences in network centrality between high and low myopia: a voxel-level degree centrality study. *Acta Radiol*. Published online February 25, 2020:0284185120902385. doi:10.1177/0284185120902385

17. Michel CM, Murray MM. Towards the utilization of EEG as a brain imaging tool. *NeuroImage*. 2012;61(2):371-385. doi:10.1016/j.neuroimage.2011.12.039

18. Michel CM, Murray MM. Towards the utilization of EEG as a brain imaging tool. *NeuroImage*. 2012;61(2):371-385. doi:10.1016/j.neuroimage.2011.12.039

19. Matusz PJ, Thelen A, Amrein S, Geiser E, Anken J, Murray MM. The role of auditory cortices in the retrieval of single-trial auditory–visual object memories. *Eur J Neurosci*. 2015;41(5):699-708. doi:https://doi.org/10.1111/ejn.12804

20. Retsa C, Matusz PJ, Schnupp JWH, Murray MM. Selective attention to sound features mediates cross-modal activation of visual cortices. *Neuropsychologia*. 2020;144:107498. doi:10.1016/j.neuropsychologia.2020.107498

21. Thelen A, Matusz PJ, Murray MM. Multisensory context portends object memory. *Curr Biol*. 2014;24(16):R734-R735. doi:10.1016/j.cub.2014.06.040

22. Turoman N, Tivadar RI, Retsa C, Maillard AM, Scerif G, Matusz PJ. The development of attentional control mechanisms in multisensory environments. *Dev Cogn Neurosci*. 2021;48:100930. doi:10.1016/j.dcn.2021.100930

23. Berchio C, Annen LC, Bouamoud Y, Micali N. Temporal dynamics of cognitive flexibility in adolescents with anorexia nervosa: A high-density EEG study. *Eur J Neurosci*. 2023;57(6):962-980. doi:10.1111/ejn.15921

24. Biria M, Tomescu MI, Custo A, et al. Visual processing deficits in 22q11.2 Deletion Syndrome. *NeuroImage Clin*. 2018;17:976-986. doi:10.1016/j.nicl.2017.12.028

25. Jan RK, Rihs TA, Kojovic N, et al. Neural Processing of Dynamic Animated Social Interactions in Young Children With Autism Spectrum Disorder: A High-Density Electroencephalography Study. *Front Psychiatry*. 2019;10:582. doi:10.3389/fpsyt.2019.00582

26. Layer N, Weglage A, Müller V, et al. Electrophysiological differences and similarities in audiovisual speech processing in CI users with unilateral and bilateral hearing loss. *Curr Res Neurobiol*. 2022;3:100059. doi:10.1016/j.crneur.2022.100059

27. Retsa C, Turpin H, Geiser E, Ansermet F, Müller-Nix C, Murray MM. Longstanding Auditory Sensory and Semantic Differences in Preterm Born Children. *Brain Topogr*. Published online November 27, 2023. doi:10.1007/s10548-023-01022-2

28. Altschuler TS, Molholm S, Butler JS, Mercier MR, Brandwein AB, Foxe JJ. The effort to close the gap: Tracking the development of illusory contour processing from childhood to

adulthood with high-density electrical mapping. *NeuroImage*. 2014;90:360-373. doi:10.1016/j.neuroimage.2013.12.029

29. Hadad BS, Maurer D, Lewis TL. The development of contour interpolation: Evidence from subjective contours. *J Exp Child Psychol*. 2010;106(2):163-176. doi:10.1016/j.jecp.2010.02.003

30. Murray MM, Herrmann CS. Illusory contours: a window onto the neurophysiology of constructing perception. *Trends Cogn Sci*. 2013;17(9):471-481. doi:10.1016/j.tics.2013.07.004

31. Mendola JD, Dale AM, Fischl B, Liu AK, Tootell RBH. The Representation of Illusory and Real Contours in Human Cortical Visual Areas Revealed by Functional Magnetic Resonance Imaging. *J Neurosci*. 1999;19(19):8560-8572. doi:10.1523/JNEUROSCI.19-19-08560.1999

32. Murray MM, Wylie GR, Higgins BA, Javitt DC, Schroeder CE, Foxe JJ. The spatiotemporal dynamics of illusory contour processing: combined high-density electrical mapping, source analysis, and functional magnetic resonance imaging. *J Neurosci Off J Soc Neurosci*. 2002;22(12):5055-5073.

33. Ringach DL, Shapley R. Spatial and Temporal Properties of Illusory Contours and Amodal Boundary Completion. *Vision Res*. 1996;36(19):3037-3050. doi:10.1016/0042-6989(96)00062-4

34. McKyton A, Ben-Zion I, Doron R, Zohary E. The Limits of Shape Recognition following Late Emergence from Blindness. *Curr Biol*. 2015;25(18):2373-2378. doi:10.1016/j.cub.2015.06.040

35. Knebel JF, Murray MM. Towards a resolution of conflicting models of illusory contour processing in humans. *NeuroImage*. 2012;59(3):2808-2817. doi:10.1016/j.neuroimage.2011.09.031

36. IBM Corp. IBM SPSS Statistics for Windows. Published online Released 2021. https://www.ibm.com/support/pages/how-cite-ibm-spss-statistics-or-earlier-versions-spss

37. Brunet D, Murray MM, Michel CM. Spatiotemporal Analysis of Multichannel EEG: CARTOOL. *Comput Intell Neurosci*. 2011;2011:e813870. doi:10.1155/2011/813870

38. Perrin F, Pernier J, Bertnard O, Giard MH, Echallier JF. Mapping of scalp potentials by surface spline interpolation. *Electroencephalogr Clin Neurophysiol*. 1987;66(1):75-81. doi:10.1016/0013-4694(87)90141-6

39. Knebel JF, Notter MP. STEN 1.0: Statistical Toolbox for Electrical Neuroimaging. Published online January 24, 2012. doi:10.5281/zenodo.1164038

40. Koenig T, Kottlow M, Stein M, Melie-García L. Ragu: A Free Tool for the Analysis of EEG and MEG Event-Related Scalp Field Data Using Global Randomization Statistics. Computational Intelligence and Neuroscience. doi:10.1155/2011/938925

41. Guthrie D, Buchwald JS. Significance Testing of Difference Potentials. *Psychophysiology*. 1991;28(2):240-244. doi:https://doi.org/10.1111/j.1469-8986.1991.tb00417.x

42. Murray MM, Brunet D, Michel CM. Topographic ERP Analyses: A Step-by-Step Tutorial Review. *Brain Topogr*. 2008;20(4):249-264. doi:10.1007/s10548-008-0054-5

43. Menendez RG de P, Andino SG, Lantz G, Michel CM, Landis T. Noninvasive Localization of Electromagnetic Epileptic Activity. I. Method Descriptions and Simulations. *Brain Topogr*. 2001;14(2):131-137. doi:10.1023/A:1012944913650

44. Grave de Peralta Menendez R, Murray MM, Michel CM, Martuzzi R, Gonzalez Andino SL. Electrical neuroimaging based on biophysical constraints. *NeuroImage*. 2004;21(2):527-539. doi:10.1016/j.neuroimage.2003.09.051

45. Michel CM, Murray MM, Lantz G, Gonzalez S, Spinelli L, Grave de Peralta R. EEG source imaging. *Clin Neurophysiol*. 2004;115(10):2195-2222. doi:10.1016/j.clinph.2004.06.001

46. Spinelli L, Andino SG, Lantz G, Seeck M, Michel CM. Electromagnetic Inverse Solutions in Anatomically Constrained Spherical Head Models. *Brain Topogr*. 2000;13(2):115-125. doi:10.1023/A:1026607118642

47. De Lucia M, Tzovara A, Bernasconi F, Spierer L, Murray MM. Auditory perceptual decision-making based on semantic categorization of environmental sounds. *NeuroImage*. 2012;60(3):1704-1715. doi:10.1016/j.neuroimage.2012.01.131

48. Retsa C, Matusz PJ, Schnupp JWH, Murray MM. What's what in auditory cortices? *NeuroImage*. 2018;176:29-40. doi:10.1016/j.neuroimage.2018.04.028

49. Townsend JT, Ashby FG. Methods of modeling capacity in simpleprocessing systems. *J Castellan F Restle Eds Cogn Theory*. 1978;3:200-239.

50. Townsend JT, Ashby FG. Stochastic modeling of elementary psychological processes. *Camb Camb Univ Press*. Published online 1983. https://psymodel.sitehost.iu.edu/papers/Townsend_and_Ashby_Part1.pdf

51. Anken J, Knebel JF, Crottaz-Herbette S, Matusz PJ, Lefebvre J, Murray MM. Cue-dependent circuits for illusory contours in humans. *NeuroImage*. 2016;129:335-344. doi:10.1016/j.neuroimage.2016.01.052

52. Anken J, Tivadar RI, Knebel JF, Murray MM. Brain mechanisms for perceiving illusory lines in humans. *NeuroImage*. 2018;181:182-189. doi:10.1016/j.neuroimage.2018.07.017

53. Foxe JJ, Murray MM, Javitt DC. Filling-in in Schizophrenia: a High-density Electrical Mapping and Source-analysis Investigation of Illusory Contour Processing. *Cereb Cortex*. 2005;15(12):1914-1927. doi:10.1093/cercor/bhi069

54. Murray MM, Foxe DM, Javitt DC, Foxe JJ. Setting Boundaries: Brain Dynamics of Modal and Amodal Illusory Shape Completion in Humans. *J Neurosci*. 2004;24(31):6898-6903. doi:10.1523/JNEUROSCI.1996-04.2004

55. Murray MM, Imber ML, Javitt DC, Foxe JJ. Boundary Completion Is Automatic and Dissociable from Shape Discrimination. *J Neurosci*. 2006;26(46):12043-12054. doi:10.1523/JNEUROSCI.3225-06.2006

56. Pegna AJ, Khateb A, Murray MM, Landis T, Michel CM. Neural processing of illusory and real contours revealed by high-density ERP mapping. *NeuroReport*. 2002;13(7):965.

57. Shpaner M, Murray MM, Foxe JJ. Early processing in the human lateral occipital complex is highly responsive to illusory contours but not to salient regions. *Eur J Neurosci*. 2009;30(10):2018-2028. doi:10.1111/j.1460-9568.2009.06981.x

58. Tivadar RI, Retsa C, Turoman N, Matusz PJ, Murray MM. Sounds enhance visual completion processes. *NeuroImage*. 2018;179:480-488. doi:10.1016/j.neuroimage.2018.06.070

59. Murray MM, Herrmann CS. Illusory contours: a window onto the neurophysiology of constructing perception. *Trends Cogn Sci*. 2013;17(9):471-481. doi:10.1016/j.tics.2013.07.004

60. Putzar L, Hötting K, Rösler F, Röder B. The development of visual feature binding processes after visual deprivation in early infancy. *Vision Res*. 2007;47(20):2616-2626. doi:10.1016/j.visres.2007.07.002

61. De Stefani E, Pinello L, Campana G, Mazzarolo M, Lo Giudice G, Casco C. Illusory Contours over Pathological Retinal Scotomas. *PLoS ONE*. 2011;6(10). doi:10.1371/journal.pone.0026154

62. Sun Y, Li F, Li H, et al. Performance of Topological Perception in the Myopic Population. *Curr Eye Res*. 2020;45(11):1458-1465. doi:10.1080/02713683.2020.1755697

63. Coren S, Ward LM, Porac C, Fraser R. The effect of optical blur on visual-geometric illusions. *Bull Psychon Soc*. 1978;11(6):390-392. doi:10.3758/BF03336863

64. Ward LM, Coren S. The effect of optically induced blur on the magnitude of the Mueller-Lyer illusion. *Bull Psychon Soc*. 1976;7(5):483-484. doi:10.3758/BF03337255

65. Yoshino A, Kawamoto M, Yoshida T, et al. Activation time course of responses to illusory contours and salient region: A high-density electrical mapping comparison. *Brain Res*. 2006;1071(1):137-144. doi:10.1016/j.brainres.2005.11.089

66. Stanley DA, Rubin N. fMRI Activation in Response to Illusory Contours and Salient Regions in the Human Lateral Occipital Complex. *Neuron*. 2003;37(2):323-331. doi:10.1016/S0896-6273(02)01148-0

67. Foxe JJ, Simpson GV. Flow of activation from V1 to frontal cortex in humans. *Exp Brain Res*. 2002;142(1):139-150. doi:10.1007/s00221-001-0906-7

68. Murray MM, Foxe JJ, Higgins BA, Javitt DC, Schroeder CE. Visuo-spatial neural response interactions in early cortical processing during a simple reaction time task: a high-density electrical mapping study. *Neuropsychologia*. 2001;39(8):828-844. doi:10.1016/S0028-3932(01)00004-5

69. Altschuler TS, Molholm S, Russo NN, et al. Early electrophysiological indices of illusory contour processing within the lateral occipital complex are virtually impervious to manipulations of illusion strength. *NeuroImage*. 2012;59(4):4074-4085. doi:10.1016/j.neuroimage.2011.10.051

70. Doniger GM, Foxe JJ, Murray MM, et al. Activation Timecourse of Ventral Visual Stream Object-recognition Areas: High Density Electrical Mapping of Perceptual Closure Processes. *J Cogn Neurosci*. 2000;12(4):615-621. doi:10.1162/089892900562372

71. Doniger GM, Silipo G, Rabinowicz EF, Snodgrass JG, Javitt DC. Impaired Sensory Processing as a Basis for Object-Recognition Deficits in Schizophrenia. *Am J Psychiatry*. 2001;158(11):1818-1826. doi:10.1176/appi.ajp.158.11.1818

72. Sehatpour P, Molholm S, Javitt DC, Foxe JJ. Spatiotemporal dynamics of human object recognition processing: An integrated high-density electrical mapping and functional imaging study of "closure" processes. *NeuroImage*. 2006;29(2):605-618. doi:10.1016/j.neuroimage.2005.07.049

73. Huang X, Hu Y, Zhou F, et al. Altered whole-brain gray matter volume in high myopia patients: a voxel-based morphometry study. *Neuroreport*. 2018;29(9):760-767. doi:10.1097/WNR.0000000000001028

74. Li Q, Guo M, Dong H, Zhang Y, Fu Y, Yin X. Voxel-based analysis of regional gray and white matter concentration in high myopia. *Vision Res*. 2012;58:45-50. doi:10.1016/j.visres.2012.02.005

75. Cheng Y, Huang X, Hu YX, et al. Comparison of intrinsic brain activity in individuals with low/moderate myopia versus high myopia revealed by the amplitude of low-frequency fluctuations: *Acta Radiol*. Published online August 9, 2019. doi:10.1177/0284185119867633

76. Yu YJ, Liang RB, Yang QC, et al. Altered Spontaneous Brain Activity Patterns in Patients After Lasik Surgery Using Amplitude of Low-Frequency Fluctuation: A Resting-State Functional MRI Study. *Neuropsychiatr Dis Treat*. 2020;16:1907-1917. doi:10.2147/NDT.S252850

77. Poulere E, Moschandreas J, Kontadakis GA, Pallikaris IG, Plainis S. Effect of blur and subsequent adaptation on visual acuity using letter and Landolt C charts: differences between emmetropes and myopes. *Ophthalmic Physiol Opt*. 2013;33(2):130-137. doi:10.1111/opo.12020

78. Radhakrishnan H, Pardhan S, Calver RI, O'Leary DJ. Effect of defocus on contrast sensitivity in myopes and non-myopes. *Ophthalmic Physiol Opt*. 2002;22(6):575-575. doi:https://doi.org/10.1046/j.1475-1313.2002.00086_12.x

79. Thorn F, Cameron L, Arnel J, Thorn S. Myopia Adults See Through Defocus Better Than Emmetropes. In: Tokoro T, ed. *Myopia Updates: Proceedings of the 6th International Conference on Myopia*. Springer Japan; 1998:368-374. doi:10.1007/978-4-431-66959-3_65

80. Anand A, Moraes C, Teng C, Liebmann J, Ritch R, Tello C. Short-duration transient visual evoked potential for objective measurement of refractive errors. *Doc Ophthalmol Adv Ophthalmol*. 2011;123:141-147. doi:10.1007/s10633-011-9289-7

81. Nakamura M, Kato K, Kamata S, Ishikawa K, Nagai T. Effect of refractive errors on multifocal VEP responses and standard automated perimetry tests in a single population. *Doc Ophthalmol*. 2014;128(3):179-189. doi:10.1007/s10633-014-9431-4

82. Garg S, Jain A, Singh KD, Kumar A. Evaluation of the effect of myopia on visual evoked potential in medical students. *Natl J Physiol Pharm Pharmacol*. 2022;12(10):1605-1605. doi:10.5455/njppp.2022.12.02067202211022022

83. Kordek D, Voda P, Young LK, Kremlacek J. Effect of Dioptric Blur on Pattern-Reversal and Motion-Onset VEPs as Used in Clinical Research. *Transl Vis Sci Technol*. 2022;11(12):7. doi:10.1167/tvst.11.12.7

Supplementary Data

Supplementary Table S2: Refraction results in the myopia group.

Right Eye				*Left Eye*				*Avg.*	*Years with*	*Age Range at First*
Sph.	*Cyl.*	*Axis*	*SRE*	*Sph.*	*Cyl.*	*Axis*	*SRE*	*SRE*	*Correction*	*Diagnosis*
-1.50	-1.00	175	-2.000	-1.75	-.75	180	-2.125	-2.063	15.00	10-15
-4.00	-.25	70	-4.125	-3.25	.00	.00	-3.250	-3.688	10.00	10-15
-1.50	.00	.00	-1.500	-2.00	-.25	120	-2.125	-1.813	15.00	16-20
-2.50	-1.25	10	-3.125	-2.50	-1.25	170	-3.125	-3.125	25.00	10-15
-3.25	.00	.00	-3.250	-3.25	-.50	160	-3.500	-3.375	17.00	10-15
-2.75	-1.00	10	-3.250	-1.50	-1.00	170	-2.000	-2.625	9.00	16-20
-1.00	.00	.00	-1.000	-1.00	-.25	110.00	-1.125	-1.063	12.00	10-15
-2.75	.00	.00	-2.750	-2.50	-.25	155	-2.625	-2.688	8.00	10-15
-2.00	-.50	120	-2.250	-3.25	-.25	145	-3.375	-2.813	13.00	10-15
-1.50	-.25	180	-1.625	-1.25	.00	.00	-1.250	-1.438	12.00	21-25
-2.25	-.50	135	-2.500	-2.50	-.50	180	-2.750	-2.625	28.00	10-15

-3.25	.00	.00	-3.250	-3.00	.00	.00	-3.000	-3.125	8.00	16-20
-1.00	-1.25	75	-1.625				-2.625	-2.125	13.00	10-15

Supplementary Table S3: Refraction results in the emmetropia group.

Right Eye				*Left Eye*				*Avg.*
Sph.	*Cyl.*	*Axis*	*SRE*	*Sph.*	*Cyl.*	*Axis*	*SRE*	*SRE*
.25	.00	.00	.250	.25	.00	.00	.250	.250
-.25	-.25	160.00	-.375	-.25	.00	.00	-.250	-.313
.00	.00	.00	.000	.25	-.50	180.00	.000	.000
-.25	-.25	120.00	-.375	-.75	-.25	90.00	-.875	-.625
-.25	-.50	110.00	-.500	-.25	-.50	40.00	-.500	-.500
.00	.00	.00	.000	.00	.00	.00	.000	.000
.00	.00	.00	.000	.00	.00	.00	.000	.000
.00	.00	.00	.000	.00	.00	.00	.000	.000
.00	.00	.00	.000	.00	.00	.00	.000	.000
-.25	.00	.00	-.250	.00	.00	.00	.000	-.125
-.25	.00	.00	-.250	.00	.00	.00	.000	-.125
.00	.00	.00	.000	.00	.00	.00	.000	.000

Source Reconstruction (222 to 290 ms)

Myopes

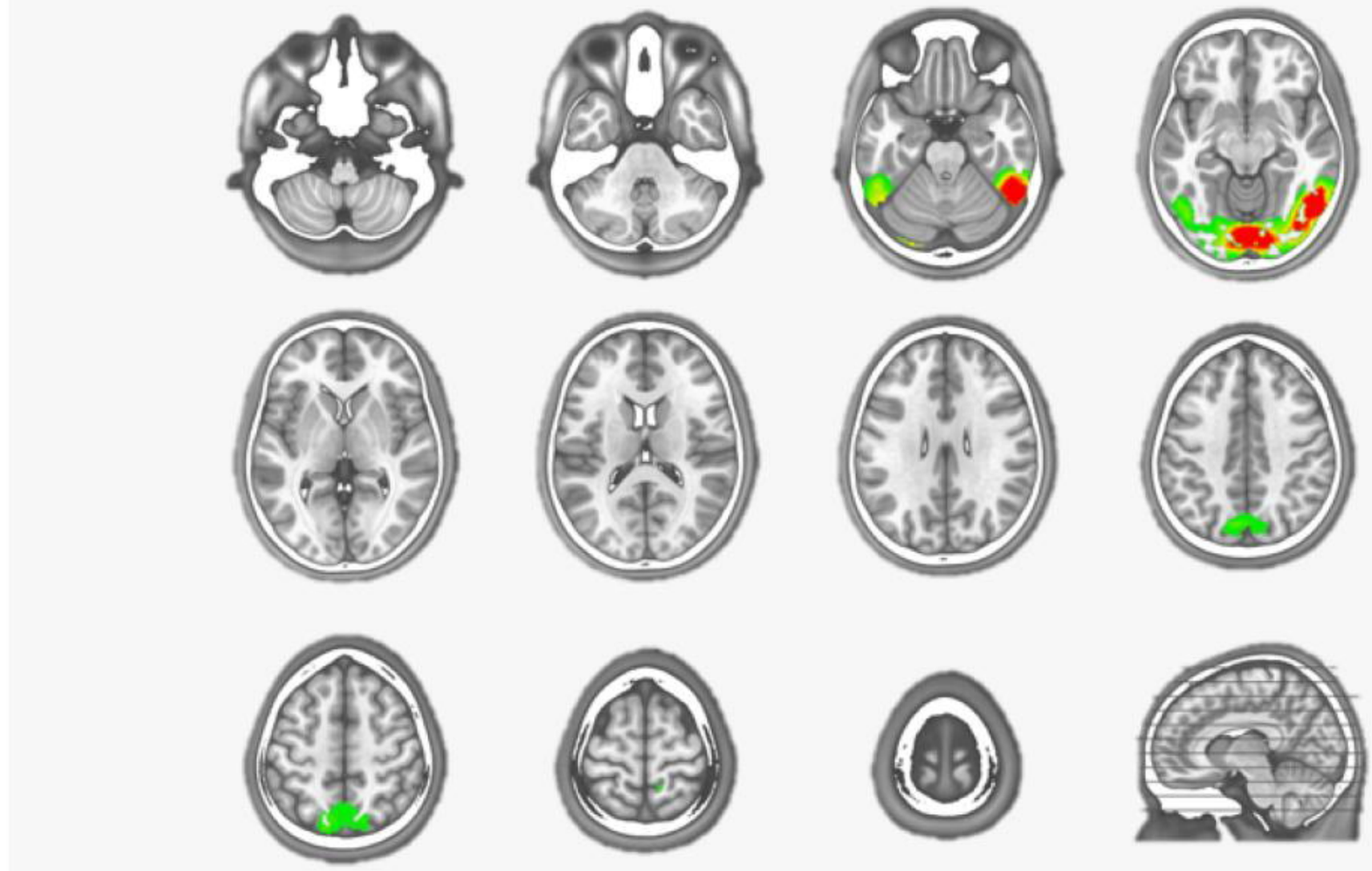

Non Myopes

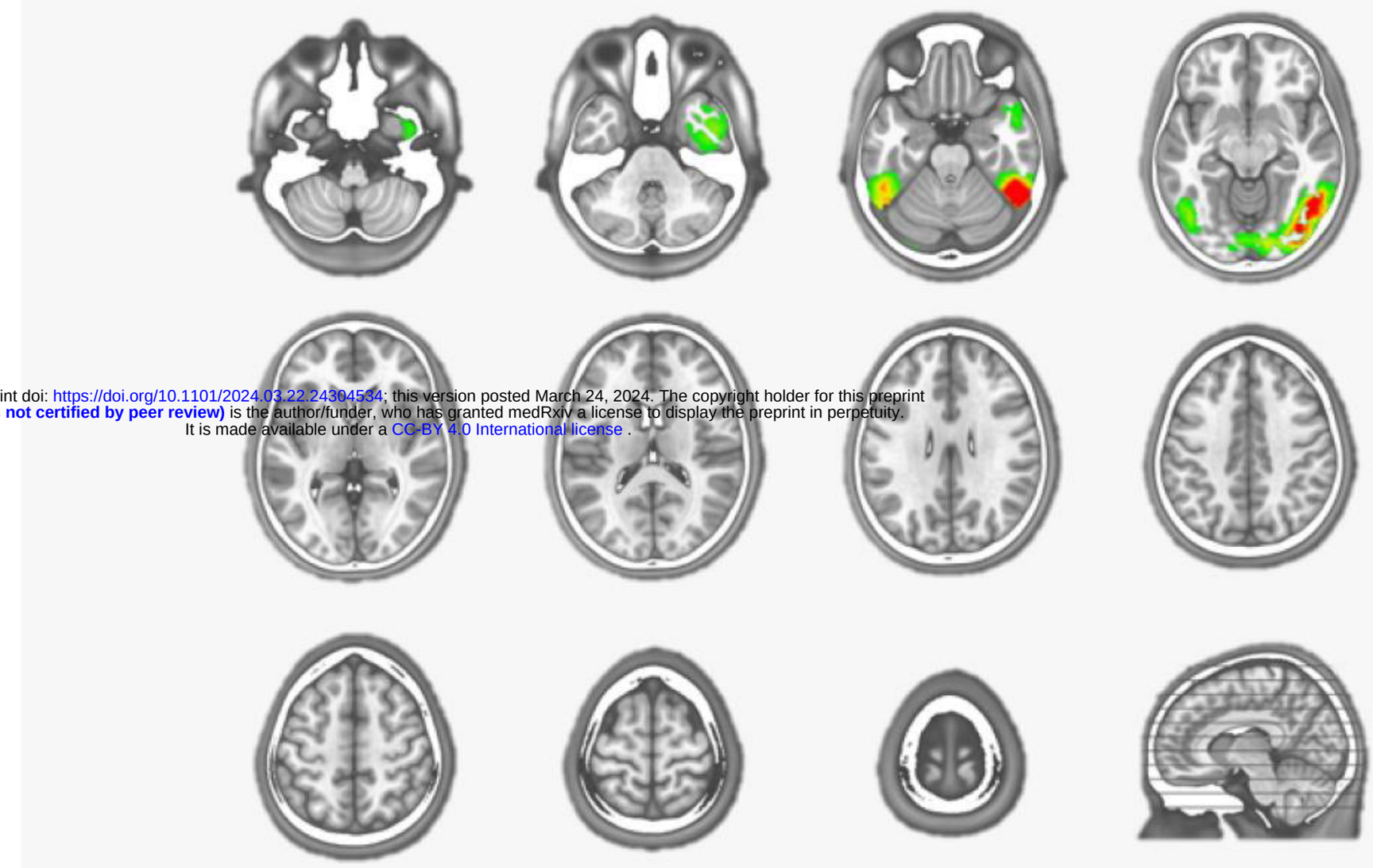

Difference

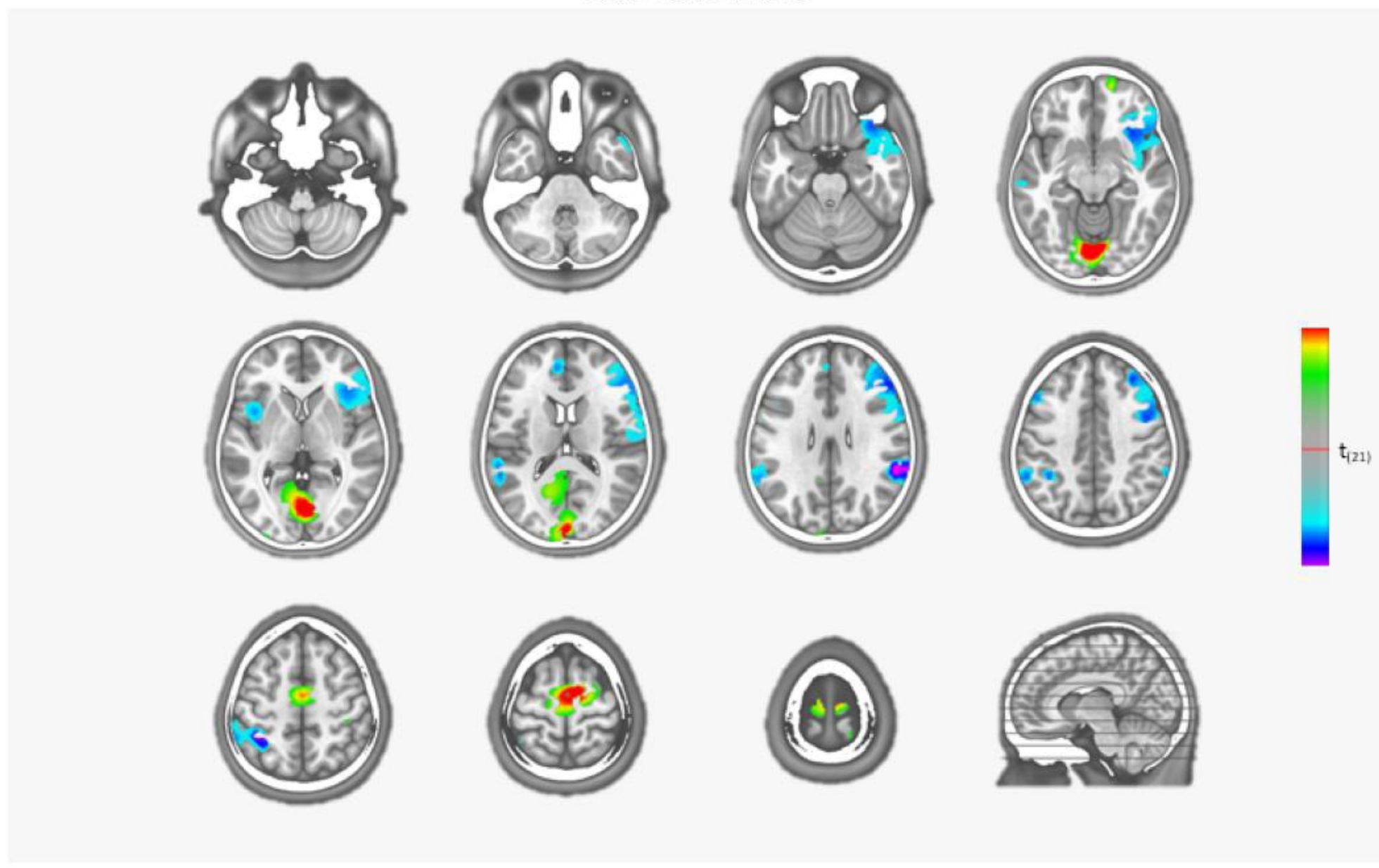

Group Differences in Duration of Stable Topographies

A. Template maps from topographic clustering

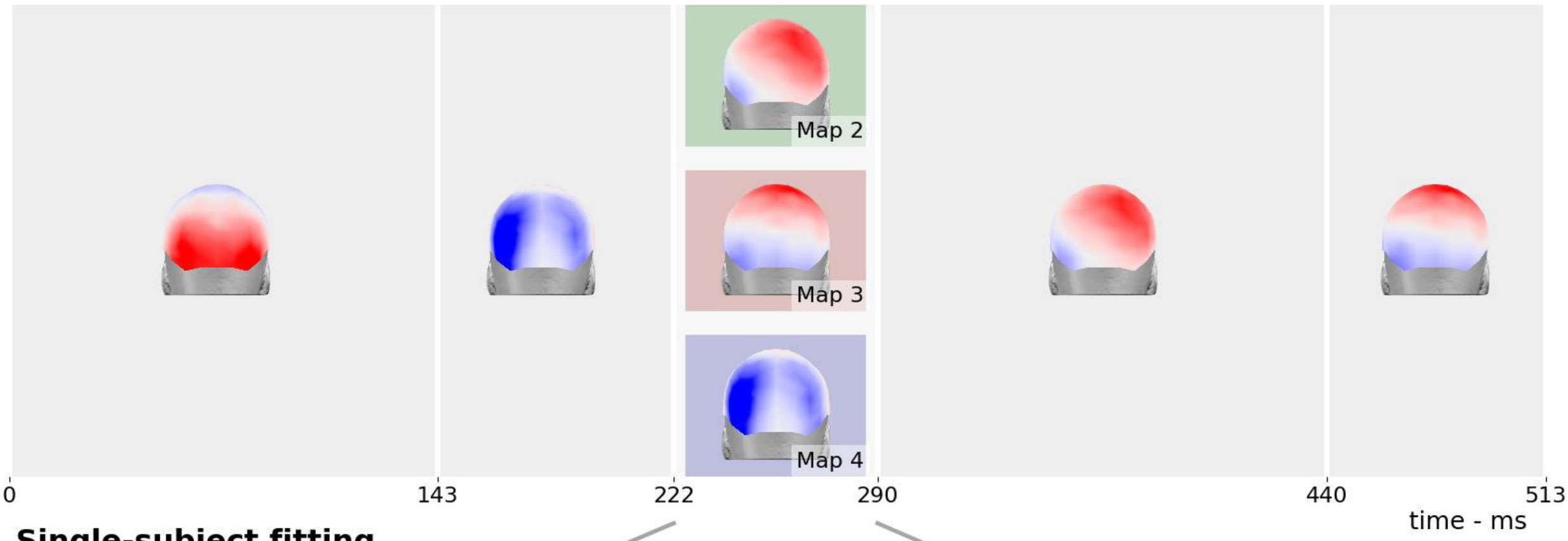

B. Single-subject fitting

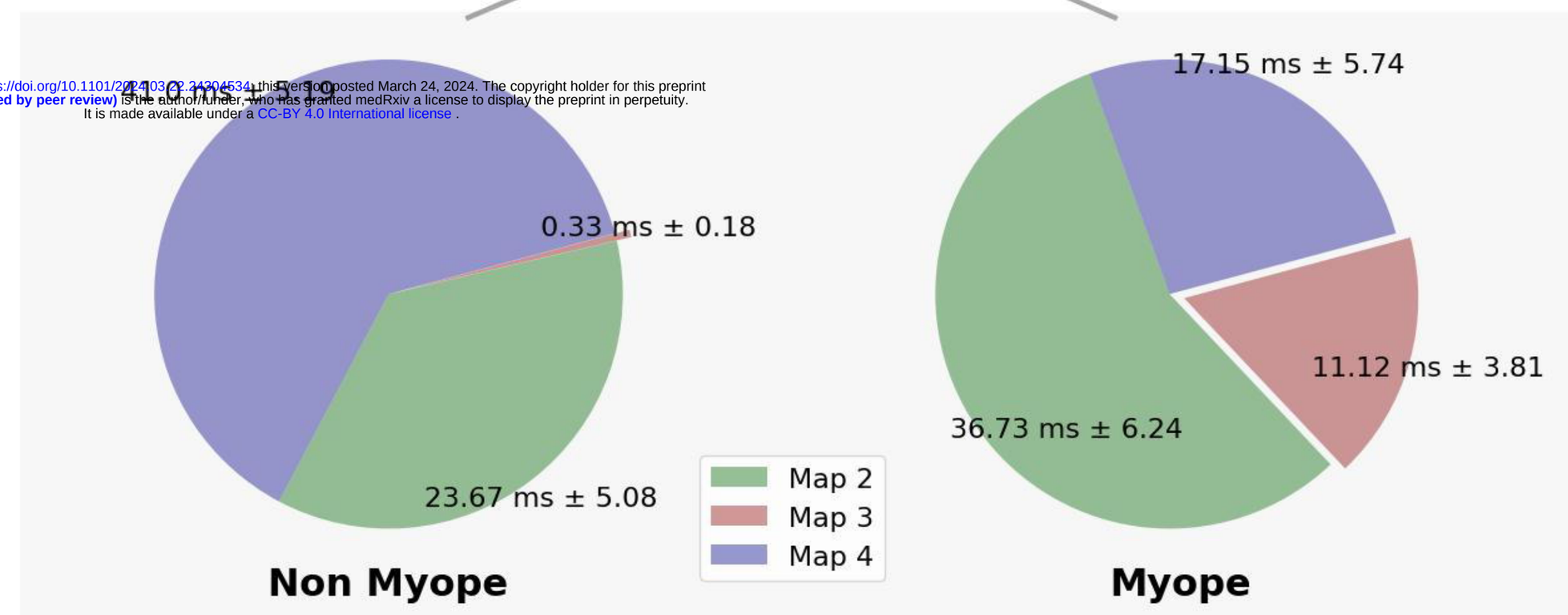

C. Classification based on template maps

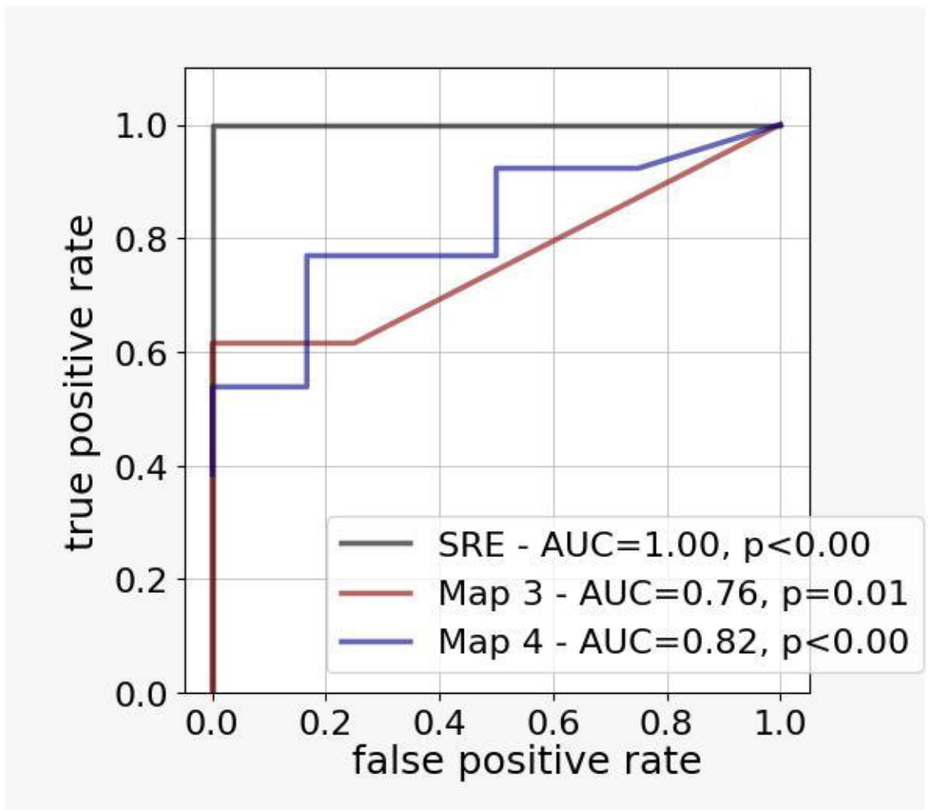

D. Correlation with SRE

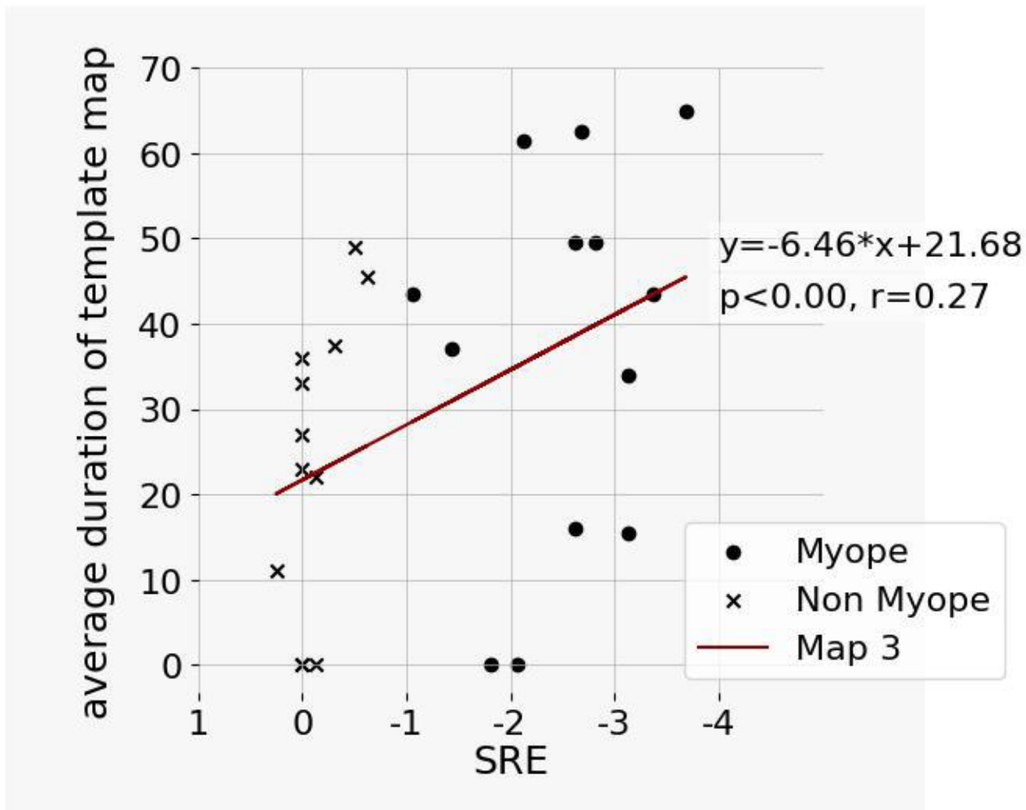

Waveforms and GFP of electrical activity at occipital electrodes

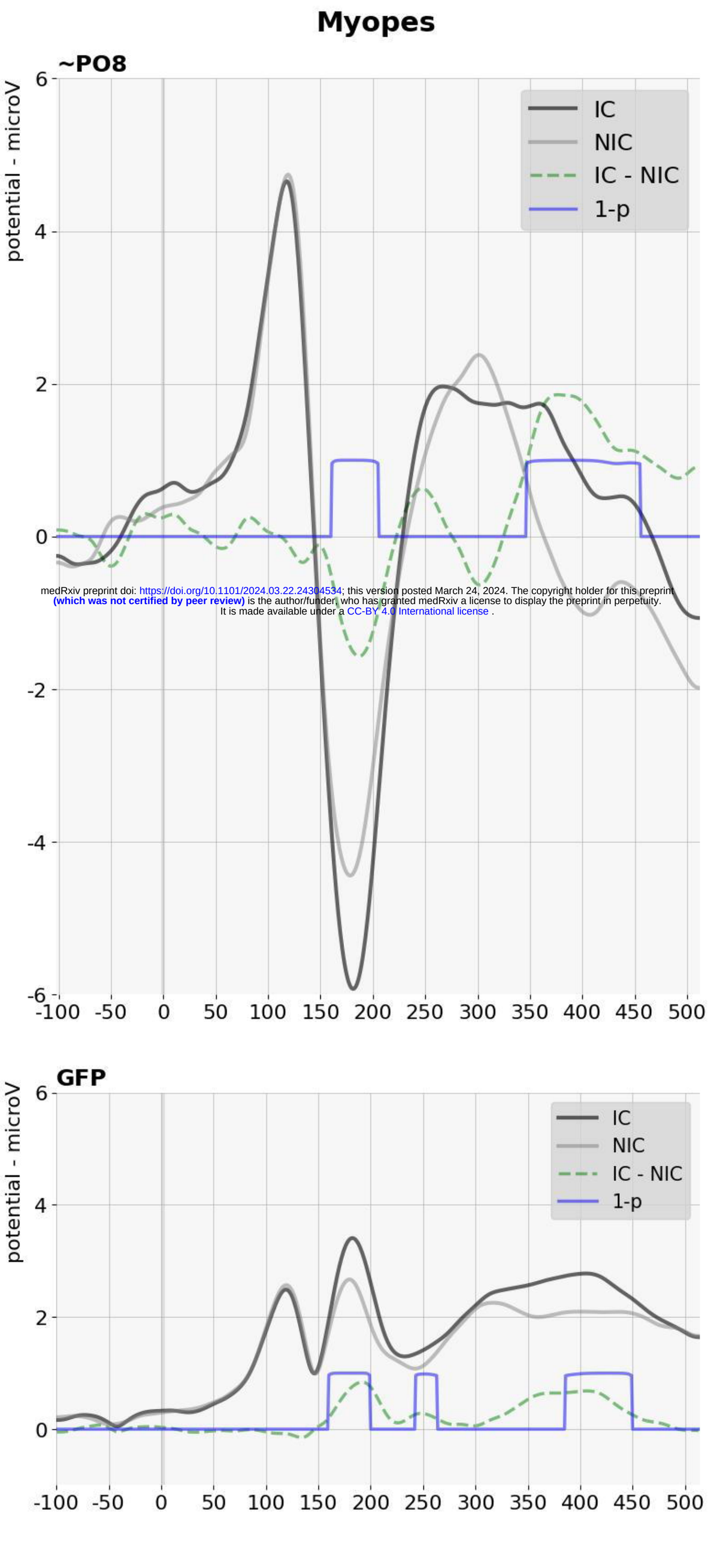

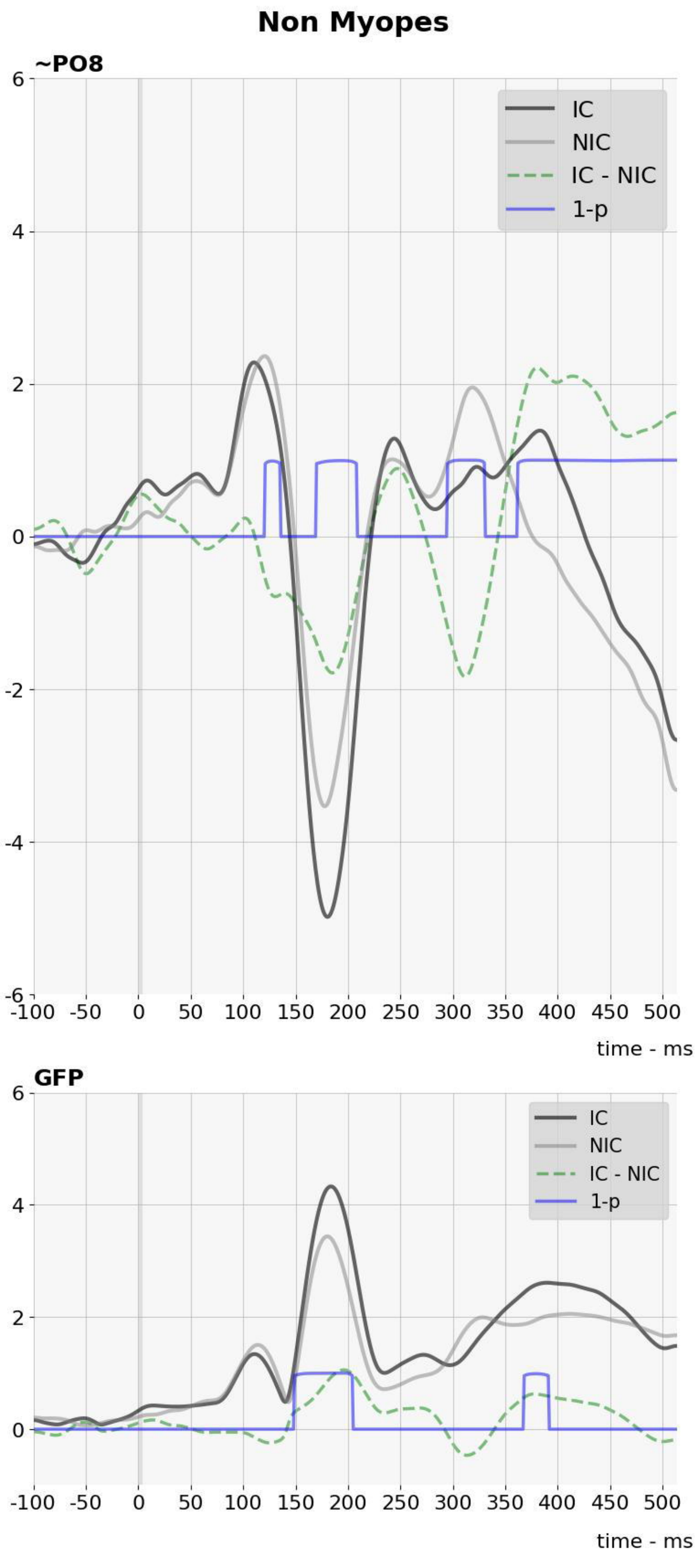

Diagram of the Experiment, Stimuli and Paradigm

Experiment

Myopes

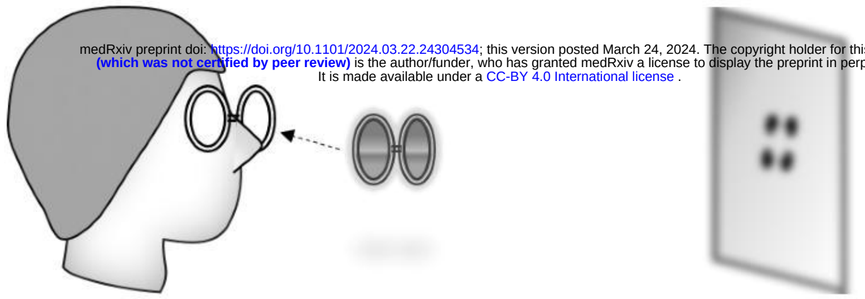

Corrected to normal vision

Eyeglasses +3 Diopters

Screen at 60cm distance

No visual correction

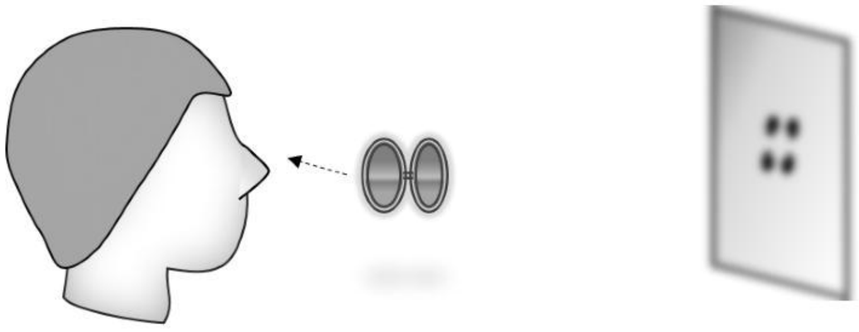

Non Myopes

Stimuli

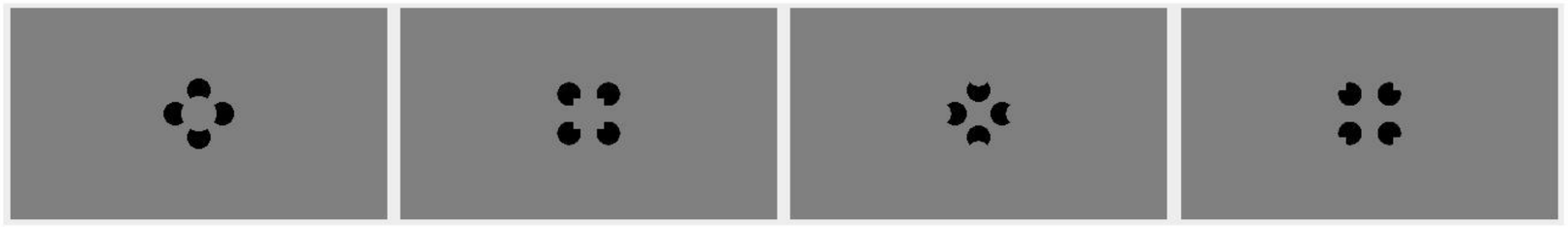

Paradigm